Discontinuous Tangential Stress in Double Wall Carbon Nanotubes

P. Puech,[1,*] H. Hubel,[2] D. J. Dunstan,[2] R. R. Bacsa,[3] C. Laurent,[3] and W. S. Bacsa[1]

[1]*Laboratoire Physique des Solides de Toulouse UMR-CNRS 5477, IRSAMC, Université Paul Sabatier, 118 Route de Narbonne, 31062 Toulouse, France*

[2]*Department of Physics, Queen Mary, University of London, Mile End Road, London, United Kingdom*

[3]*CIRIMAT-LCMIET, UMR CNRS 5085, Université Paul Sabatier, 118 Route de Narbonne, 31077 Toulouse cedex 4, France*

(Received 8 January 2004; published 27 August 2004)

We have examined the stability of double wall carbon nanotubes under hydrostatic pressures up to 10 GPa. The tangential optical phonon mode observed by inelastic light scattering is sensitive to the in-plane stress and splits into a contribution associated with the external and internal tube. While the pressure coefficient from the external tube is the same as in single wall carbon nanotubes, the pressure coefficient from the internal tube is found to be 45% smaller. The phonon band from the external tube broadens considerably with applied pressure in contrast with the phonon band of the internal tube which stays constant. These pressure dependent phonon shifts of the external and internal tubes and the contrasting phonon line broadening are explained by the elastic continuum shell model which takes into account both the continuous radial and discontinuous tangential stress components.

DOI: 10.1103/PhysRevLett.93.095506 PACS numbers: 61.46.+w, 63.22.+m, 78.30.Na, 78.67.–n

Carbon nanotubes (CNTs) are one dimensional cage structures with exceptional properties. The closed cylindrical wall protects the inside from the environment. The excellent mechanical properties of curved graphite sheets lead to a high Young's modulus [1–3] attractive for a number of applications such as force sensors, actuators, nanofluidic components or reinforcement of composites [4,5]. Load transfer from matrix to CNTs plays a key role in the mechanical properties of composite [6]. The behavior of multi wall CNTs (MWCNTs) under tensile strain is complicated [7,8]. Multiple fragmentations and buckling [9] of MWCNTs in a polymer matrix have been observed and theoretically studied [10,11]. MWCNTs are also of interest for micro and nanofluidic applications where nanotubes may provide flexible channels and injectors for functional nanodevices. The behavior of MWCNTs under stress is in this context an important issue. We provide experimental evidence for the discontinuous stress in double wall CNTs (DWCNTs) which gives us the opportunity to distinguish between the discrete model and continuous shell model.[12]

The mechanical behavior of CNTs can be studied non-invasively by observing their behavior under hydrostatic pressure and monitor the phonons by inelastic light scattering [13,14]. DWCNTs give us the unique opportunity to distinguish the contributions from external and internal tubes. For ropes of single wall CNTs (SWCNTs) with tube radius of 0.7 nm, the optical phonon band shifts linearly with applied hydrostatic pressure (pressure coefficient: 5.8 cm^{-1}/GPa) and shows a transition at 1.7 GPa [14]. At higher pressures, it was concluded using empirical force calculations that the nanotubes deform from a cylindrical into an ellipsoidal shape [14–18]. The pressure coefficient of the optical phonon band is 7-12 cm^{-1}/GPa below the transition and tends to the value for graphite (4.7 cm^{-1}/GPa) after the transition [19]. Reich et al. [20] have studied the shear strain for SWCNTs under hydrostatic pressure. The lack of the graphite band splitting was explained by the averaging of the effects due to the phonon polarization. The different pressure coefficients for SWCNTs and MWCNTs was described by Thomsen *et al.* [21] by introducing a radius dependent stress tensor.

In this Letter, we report the hydrostatic pressure dependence of the optical phonon band of the internal and external tubes of narrow diameter DWCNTs. We use the elastic continuum shell model to explain quantitatively the pressure coefficient and the differences in broadening of the optical phonon band for the internal and external tubes. We propose a model that explains the observed stress behavior of MWCNTs and resolve open questions on the stress condition between different tube walls.

The DWCNTs were prepared by the catalytic chemical vapour deposition method. Selective reduction at 1000 °C in a methane-hydrogen (18% CH4) atmosphere of a solid solution of a transition metal oxide (CoO) and an insulating oxide (MgO) led to the formation of small diameter CNT with one to four walls; for more details see Refs. [22,23]. After the reaction, the unreacted Co and MgO were dissolved in dilute (3.7%) hydrochloric acid and CNT were recovered. High-resolution electron microscopy images showed the presence of individual and small bundles of DWCNTs with radius ranging from 0.3 to 1.5 nm. The tubes were single, double or triple walled with about 70% of DWCNTs and a few four wall tubes. A significant fraction of DWCNTs had internal radius smaller than 0.5 nm.

All Raman spectra were recorded at room temperature using a Renishaw Raman microprobe instrument. The scattered light was collected in backscattering geometry. A ×20 microscopic lens was used to focus the laser beam

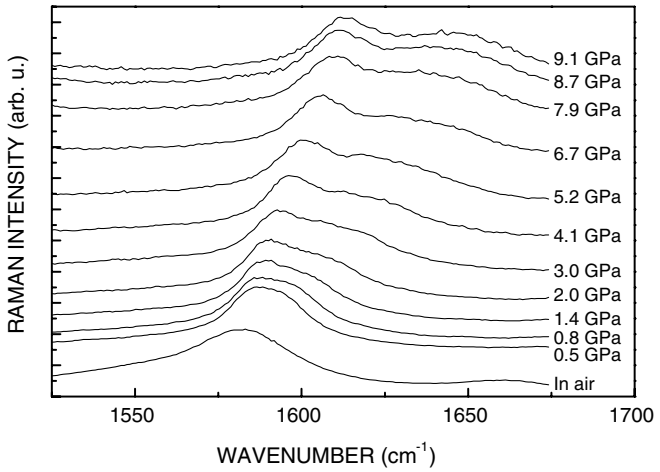

FIG. 1. Raman spectra of double wall CNT in the region of optical mode at different hydrostatic pressure.

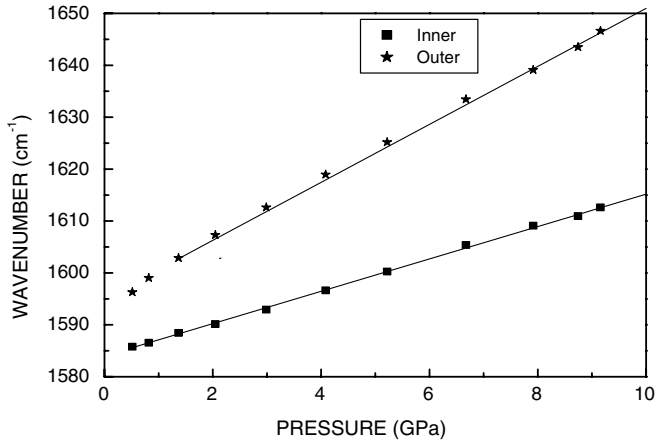

FIG. 2. Frequencies deduced from the fitting of the spectra reported in Fig. 1.

(633 nm) on the sample inside the pressure cell. The high-pressure Raman measurements were performed in a diamond anvil cell with a 4:1 mixture by volume of methanol-ethanol as the pressure-transmitting medium. The pressure chamber was defined by the volume of a 200 μm diameter hole in a steel gasket (thickness of 100 μm). The pressure was monitored using the luminescence of a ruby chip inside the cell. The DWCNTs were dispersed by sonication in the pressure medium prior to loading.

The Raman spectra recorded in the high frequency range at different hydrostatic pressures are shown in Fig. 1. We fitted (nonlinear least square) the spectra with two Lorentzians and a constant background. Figure 2 plots the energy and Fig. 3 plots the line width of the two bands as a function of pressure. In Fig. 1 we see that as the pressure is increased, a second band appears. Figure 2 shows the linear pressure dependence of the two bands (5.59 cm^{-1}/GPa, 3.11 cm^{-1}/GPa). A detailed study on graphite has shown that the optical phonon band shifts slightly sublinearly with a pressure coefficient in the range $4.7 - 4.8$ cm^{-1}/GPa and has a constant line width (15 cm^{-1}) below 9 GPa [24]. The pressure coefficients of DWCNT's differ significantly from those of graphite. The spectral position of the G band in air is 1583 cm^{-1}. This value is compatible if one includes the effect of the pressure-transmitting medium [19,25]. In the following, we do not take into account the low pressure values; they do not influence our conclusions.

In Fig. 2, the pressure coefficient is comparable to what has been found for SWCNTs (5.8 cm^{-1}/GPa) after the phase transition which is attributed to the change from circular to elliptical shape. We note that the pressure coefficient depends on the diameter and as a result on the diameter distribution of the sample. The second band which splits off shifts at a much lower rate (3.11 cm^{-1}/GPa) and is the lowest pressure coefficient found for carbon nanostructures [19]. It is interesting to note that the line width of the first band remains constant (20 cm^{-1}) while the line width of the second band increases linearly up to 5 GPa and saturates at higher pressure (50 cm^{-1}). We attribute the first band with the low pressure coefficient to the internal tube. The external tube reduces the pressure on the internal tube and as a result the pressure coefficient is expected to be reduced.

While the phase transition in SWCNTs has been identified as deformation of the cylinder shape, the presence of the internal wall is expected to reduce the deformations. Tight binding simulations and local density approximation calculations confirmed the consistency with the elastic continuum shell model (for example, see [26]). In order to explain the lower pressure coefficient of the internal tube in DWCNTs, we have used the elastic continuum shell model [19,21,27]. For the pressure dependence of a single shell with a finite wall width we have:

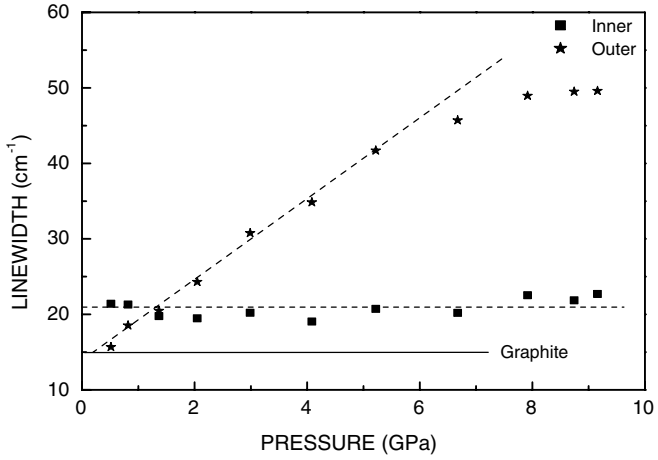

FIG. 3. Linewidth of the Lorentzians used for the fitting of the spectra reported in Fig. 1. Dashed lines are guide-eyes. Graphite value is taken from Ref. [24]

$$\sigma_{rr} = -A\left(1 - \frac{B}{r^2}\right), \sigma_{\theta\theta} = -A\left(1 + \frac{B}{r^2}\right) \text{ and } \sigma_{zz} = -A,$$

where σ is the stress tensor and r, θ and z are the corresponding cylindrical coordinates. In the case of a SWCNT, the constants A and B are determined by the boundary conditions with an outside pressure $-p$ and the inside pressure is zero. A and B are positive functions of the external radius R_2 and the internal radius R_1. If we assume a continuous stress component in radial direction and a positive B, the stress component in the tangential direction $\sigma_{\theta\theta}$ increases continuously as r decreases and there is no splitting due to internal and external tubes. The fact that we observe two bands indicates that we must take into account the pressure reduction on the internal tube. We also need to explain the low value of the pressure coefficient for the internal tubes. For DWCNTs the helicity of the tubes is necessarily different and in general incommensurate. There is no atomic alignment between the two walls and the continuity of the tangential component of the stress tensor is not established. We consider two cylinders and we assume a discontinuity of the tangential and axial stress components. In this case, the axial and tangential components change abruptly to a lower value when going from the external tube to the internal tube, giving rise to two bands. When considering two cylinders with an intermediate medium between them and denoting the outside pressure $-p$ at R_2 and $-p_i$ for the medium between the two tubes at R_i and 0 on the inside at R_1, we can determine four constants. A_{ex} and B_{ex} for the external and A_{in}, B_{in} for the internal tube:

$$A_{\text{ex}} = \frac{R_2^2 p - R_i^2 p_i}{R_2^2 - R_i^2} \quad \text{and}$$

$$B_{\text{ex}} = \frac{p - p_i}{\frac{p}{R_i^2} - \frac{p_i}{R_2^2}} A_{\text{in}} = \frac{R_i^2}{R_i^2 - R_1^2} p_i \quad \text{and} \quad B_{\text{in}} = R_1^2$$

We find the value for p_i through minimization of the strain energy. We take the strain energy of an elementary element and integrate over the two cylinders leading to:

$$p_i = \frac{\frac{R_2^2}{R_2^2 - R_i^2}(5 - 4\nu)}{3R_i^2\left(\frac{1}{R_2^2 - R_i^2} + \frac{1}{R_i^2 - R_1^2}\right)(1 - 2\nu) + 2\left(\frac{R_2^2}{R_2^2 - R_i^2} + \frac{R_1^2}{R_i^2 - R_i^1}\right)(1 + \nu)} p$$

where $\nu = 0.12$ is the Poisson's ratio and where the thickness of the wall at 0.34 nm as in Ref. [21]. We show in Fig. 4 the tangential stress for both external and internal tubes as a function of R_i.

We find that the result is largely independent of the Poisson's ratio in the range found in the literature [0.12-0.28] [1,28]. The tangential stress increases with increasing tube radius for the external tube. The tangential stress is 1.5 larger than the hydrostatic pressure for the external tube which leads to a larger shift than in graphite with $R_i = 0.7$ nm. The influence of the diameter distribution on the phonon integrated line width gives new insight. The sample contains DWCNTs with a different internal and external radius. At 0 GPa pressure, all the tubes have a given phonon frequency. The phonon pressure coefficient for smaller diameter tubes is smaller ($-1.3p$) than for large diameter tubes ($-2p$)(Fig. 4). Consequently, the peak originating from all the external tubes broadens with increasing hydrostatic pressure.

We find that the tangential stress is more or less constant for the internal tube and smaller than for the external tube. The value found close to -0.8 p is lower than the hydrostatic pressure leading to a smaller pressure coefficient than for graphite. By considering two shells we can explain the reduction of the pressure dependence for the internal nanotube. The tangential stress of the internal tube does not change with radius in the range of the DWCNT distribution and as a consequence the contribution from the internal tubes does not broaden with applied pressure.

We conclude that the elastic continuum model with two shells explains both frequency shift and broadening for internal and external tubes. The proposed model shows that DWCNTs do not behave like a homogeneous medium. We show that the discontinuity between the walls is necessary to explain the observed stress-strain behavior.

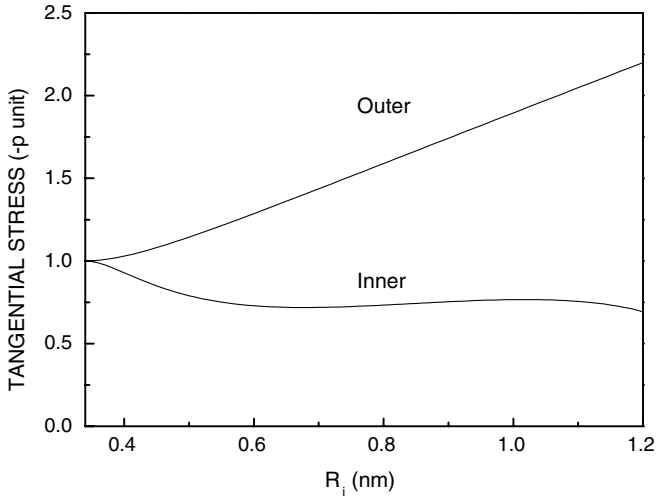

FIG. 4. Tangential stress ($\sigma_{\theta\theta}/-p$) at the surface of both external and internal tube for an intermediate radius ranging from 0.34 (no vacuum inside, $R_1 = 0$ nm and $R_2 = 0.68$ nm) to 1.2 nm ($R_1 = 0.86$ nm and $R_2 = 1.54$ nm).

In the discrete model, the wall thickness is not taken into account. We connect the two approaches and show how the wall thickness can be introduced while preserving the hypothesis of discontinuity between the walls.

In summary, we have investigated the mechanical behavior of DWCNTs under pressure by observing under hydrostatic pressure their tangential phonon modes. We are able to measure the pressure reduction on the internal tube, following the spectroscopic signature of the external and internal tubes. Our observation of the optical phonon of the external and internal tube under hydrostatic pressure are consistent with the elastic continuum shell model if we allow a discontinuity of the tangential stress components between the two tubes. This discontinuity related to the weak interlayer interaction, has important consequences for the applications of DWCNTs such as in the emerging field of nanofluidics, actuators, and reinforcement of polymers.

*Electronic address: Pascal.Puech@lpst.ups-tlse.fr

[1] J. P. Lu, J. Phys. Chem. Solids **58**, 1649 (1997).
[2] M. M. J. Treacy, T. W. Ebbesen, and J. M. Gibson, Nature (London) **381**, 678 (1996).
[3] J. Salvetat, G. Briggs, J. Bonard, R. Bacsa, A. Kulik, T. Stckli, N. A. Burnham, and L. Forŕ, Phys. Rev. Lett. **82**, 944 (1999).
[4] M. S. Dresselhaus, G. Dresselhaus, and P. Avouris, *Carbon Nanotubes: Synthesis, Structure, Properties and Applications* (Springer Verlag, Berlin, 2001), 1st ed.
[5] P. J. F. Harris, *Carbon Nanotubes and Related Structures* (Cambridge University Press, Cambridge, England 2002), 1st ed.
[6] J. Salvetat, J. Bonard, N. Thomsen, A. Kulik, L. Ferŕo, W. Benoit, and L. Zuppiroli, Appl. Phys. A **69**, 255 (1999).
[7] M. Yu, B. Files, S. Arepalli, and R. Ruoff, Phys. Rev. Lett. **84**, 5552 (2000).
[8] J. Cumings and A. Zettl, Science **289**, 602 (2000).
[9] H. Wagner, O. Lourie, Y. Feldman, and R. Tenne, Appl. Phys. Lett. **72**, 188 (1998).
[10] B. Yakobson, Appl. Phys. Lett. **72**, 918 (1998).
[11] L. Schadler, S. Giannaris, and P. Ajayan, Appl. Phys. Lett. **73**, 3842 (1998).
[12] B. Galanov, S. Galanov, and Y. Gogotsi, J. Nanoparticle Research, **207** (2002).
[13] U. Venkateswaren, A. Rao, E. Richter, M. Menon, A. Rinzler, R. Smaller, and P. Eklund, Phys. Rev. B **59**, 10928 (1999).
[14] M. Peters, L. McNeil, J. Lu, and D. Kahn, Phys. Rev. B **61**, 5939 (2000).
[15] T. Yildirim, O. Glseren, C. Kilic, and S. Ciraci, Phys. Rev. B **62**, 12648 (2000).
[16] A. K. Sood, P. V. Teresdesai, D. V. S. Muthu, R. Sen, A. Govindaraj, and C. N. R. Rao, Phys. Status Solidi B **215**, 393 (1999).
[17] D. Kahn and J. Lu, Phys. Rev. B **60**, 6535 (1999).
[18] S. A. Chesnokov, V. A. Nalimova, A. G. Rinzler, R. E. Smalley, and J. E. Fischer, Phys. Rev. Lett. **82**, 343 (1999).
[19] J. Sandler, M. S. P. Shaffer, A. H. Windle, M. P. Halsall, M. A. Montes-Moran, C. A. Cooper, and R. J. Young, Phys. Rev. B **67**, 035417 (2003).
[20] S. Reich, H. Jantoljak, and C. Thomsen, Phys. Rev. B **61**, R13389 (2000).
[21] C. Thomsen, S. Reich, H. Jantoljak, I. Loa, K. Syassen, M. Burghard, G. Duesberg, and S. Roth, Appl. Phys. A **69**, 309 (1999).
[22] R. Bacsa, C. Laurent, A. Peigney, W. Bacsa, T. Vaugien, and A. Rousset, Chem. Phys. Lett. **323**, 566 (2000).
[23] E. Flahaut, R. Bacsa, A. Peigney, and C. Laurent, Chem. Commun. (Cambridge) **12**, 1442 (2003).
[24] M. Hanfland, H. Beister, and K. Syassen, Phys. Rev. B **39**, 12598 (1989).
[25] J. Wood, Q. Zhao, M. Frogley, E. Meurs, A. Prins, T. Peijs, D. Dunstan, and H. Wagner, Phys. Rev. B **62**, 7571 (2000).
[26] S. Reich, C. Thomsen, and P. Ordejon, Phys. Rev. B **65**, 153407 (2002).
[27] A. Boresi and R. Schmidt, *WIE Advanced Mechanics of Materials* (John Wiley & Sons, New York, 2003), 6th ed..
[28] D. Sanchez-Portal, E. Attacho, and M. Solet, Phys. Rev. B **59**, 12678 (1991).